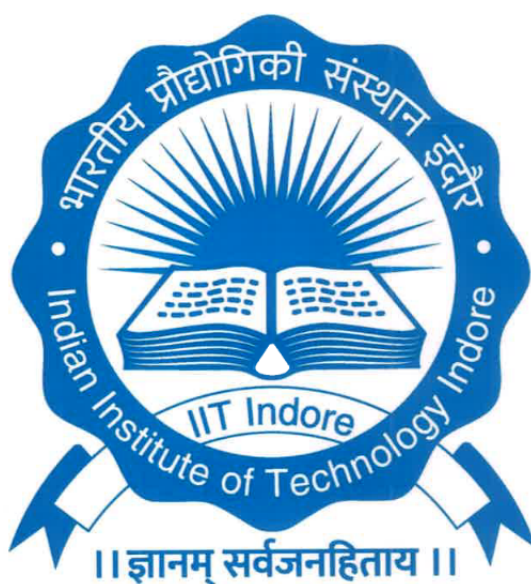


Investigating the Equation of Hydrostatic Equilibrium under the Modified Newtonian Dynamics

M.Sc. Thesis

by

Anshul



DEPARTMENT OF MATHEMATICS
INDIAN INSTITUTE OF TECHNOLOGY INDORE
MAY 2025

Hydrostatic Equilibrium under MOND

A THESIS

*Submitted in partial fulfillment of the
requirements for the award of the degree
of*

Master of Science

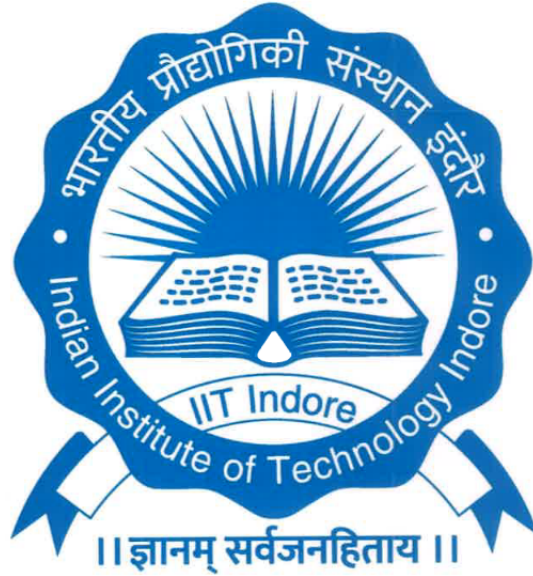
by

Anshul

(Roll No. 2303141004)

Under the guidance of

Dr. Santanu Manna and Dr. Narendra Nath Patra



DEPARTMENT OF MATHEMATICS
INDIAN INSTITUTE OF TECHNOLOGY INDORE

MAY 2025

INDIAN INSTITUTE OF TECHNOLOGY INDORE
CANDIDATE'S DECLARATION

I hereby certify that the work which is being presented in the thesis entitled "**Investigating the Equation of Hydrostatic Equilibrium under the Modified Newtonian Dynamics**" in the partial fulfillment of the requirements for the award of the degree of **Master of Science** and submitted in the **Department of Mathematics, Indian Institute of Technology Indore**, is an authentic record of my own work carried out during the time period from July 2024 to May 2025 under the supervision of **Dr. Santanu Manna**, Associate Professor, Department of Mathematics, IIT Indore, and **Dr. Narendranath Patra**, Assistant Professor, Department of Astronomy, Astrophysics and Space Engineering, IIT Indore.

The matter presented in this thesis by me has not been submitted for the award of any other degree of this or any other institute.

Anshul 23/05/2025

Signature of the student

(Anshul)

This is to certify that the above statement made by the candidate is correct to the best of my knowledge.

 23/05/2025
Signature of Thesis Supervisor

Dr. Santanu Manna


Narendranath Patra
23.05.2025
Signature of Thesis Co-supervisor

Dr. Narendranath Patra

Anshul will appear for his M.Sc. Oral Examination on **29th May 2025**.

Narendranath Patra
23.05.2025
Signature of Thesis Supervisors

Dr. Manna & Dr. Patra

 23/05/2025
Signature of DPGC Convener

Dr. Vijay Kumar Sohani

Acknowledgements

First and foremost, I would like to express my gratitude to my supervisors, Dr. Santanu Manna and Dr. Narendranath Patra. I am deeply appreciative of the opportunity they provided me to work under their esteemed guidance and for their confidence in my abilities. Their knowledge, patience, and support throughout the duration of the project were crucial in shaping my research direction and refining my approach.

I am thankful to the members of the Applied Mathematics and Geomechanics Lab (AMG) and the Galaxy Research and Radio Instrumentation Lab (GRRIL) for their consistent assistance and insightful discussions. I am particularly grateful to Ms. Manasa Bhat, Mr. Rahul Som, and Mr. Atharva Mirashi for their generous help and valuable suggestions, which significantly contributed to my work. I also extend my thanks to my friends, whose constant encouragement and moral support were a great source of strength, especially during the challenging phases of this project.

Lastly, I would like to express my gratitude to my parents, who always believed in me. Their unwavering faith in my ability, as well as their persistent support, has been a driving force behind what I have accomplished.

Abstract

This thesis investigates the vertical structure of galactic discs by considering the hydrostatic equilibrium under the Modified Newtonian Dynamics (MOND). The observed discrepancies between the galactic rotation curves and the predictions of Newtonian gravity without dark matter inspired me to delve into the investigation of Modified Newtonian Dynamics as an alternative framework. This study examines how MOND influences the vertical distribution of baryonic matter in galactic discs.

This thesis derives the classical equation of hydrostatic equilibrium in the Newtonian regime and constructs a modified second-order differential equation for corrections in the deep-MOND regime. The gravitational influence of stars, atomic hydrogen, and molecular hydrogen is considered to construct a self-consistent model for the vertical density distribution. The study further emphasizes scale height as a diagnostic tool for comparing the theoretical predictions with observational data from galaxies.

The work presents a numerical analysis and graphical representations of scale height under various assumptions, which highlight the significant deviations introduced by MOND. The findings provide insights into whether MOND can account for the observed vertical structure of galactic discs without invoking dark matter halos. By evaluating the implications of modified dynamics in the vertical structure of galaxies, this thesis contributes to the broader discourse on alternative gravity theories and their observational consequences.

Contents

1	Introduction	1
1.1	Literature survey	1
1.2	Recent development	2
1.3	Newton's law of gravitation	3
1.4	Galaxy dynamics	3
1.5	Rotation curve	4
1.6	Scaleheight	5
1.7	Dark matter halo	6
1.8	Interstellar medium	6
1.9	Half-width at half maximum	7
2	Galaxy Structure	9
2.1	Radial structure	10
2.2	Vertical structure	11
2.3	Hydrostatic equilibrium	12
3	Formulation of Model	15
3.1	Assumptions of hydrostatic equilibrium	16
3.2	Establishment of the equation	16
3.3	Methods for solving equations	17
3.3.1	Solution of equations	17
3.3.2	Parameters used	18
3.4	Mathematical formulation	18

3.5 Observations	21
4 Formulation of MOND	23
4.1 Introduction	23
4.2 Mathematical framework	24
4.2.1 Assumption of the modified Poisson equation	24
4.2.2 Expression for fictitious dark matter	25
4.2.3 Expression for surface density of fictitious dark matter	26
4.2.4 Scale height of 1-D planar mass layer	27
4.2.5 Gravitational potential in axisymmetric thin discs	29
5 Numerical Implementation and Result	33
5.1 DOPRI5	33
5.2 DOP853	36
5.3 Results	37
6 Conclusion	41
Future Scope	43
Bibliography	45

List of Figures

1.1 Structure of galaxy	4
1.2 Rotation curve of galaxy	5
1.3 Dark matter halo	6
1.4 Half-width at half maximum	7
2.1 Hydrostatic equilibrium	13
5.1 Plot of surface density vs radius for HI	37
5.2 Plot of surface density vs radius for stars	38
5.3 Plot of density vs height	38
5.4 Plot of surface density vs R	39

Chapter 1

Introduction

1.1 Literature survey

The current leading model of the universe, known as Λ CDM (Lambda Cold Dark Matter), consists of two dominant components whose existence is inferred almost entirely from the astronomical data. First, we know about the "dark energy" that Einstein himself thought about. This dark energy makes up a huge chunk, about 70%, of everything in the universe. This is making the universe spread out faster and faster, and we know this because we have seen how quickly distant exploding stars are moving away from us. The second component we know is the "cold dark matter." The cold dark matter makes up about 25% of the universe by Brada and Milgrom [1]. It mainly interacts with stars and planets (which is only about 5% of everything) through gravity. It is called cold because it was moving slowly way back when the universe was young, and it stopped bumping into light particles. Because it was slow, its gravity was strong enough at pulling things together, and this helped galaxies and other big structures start forming early in the universe, as discussed by Sanders [2]. It also helps explain a puzzle: when we look at galaxies and groups of galaxies, they seem to have much more gravity pulling them together than we can account for just by looking at the stars and gas we can actually see.

There is a common assertion within the scientific community that the evi-

dence for the standard model of the universe is so strong that other ideas are mostly set aside. This strong belief continues, even though the lab experiments have not yet detected the dark matter particles that scientists thought were most likely to be found. Despite these experiments yielding no such discoveries, the search continues. So, in view of this, the main idea (called Λ CDM) has become the accepted belief discussed by Angus [3], and Milgrom [4].

1.2 Recent development

However, there is an important idea that goes against this, called the Modified Newtonian Dynamics or the theory of Modified Gravity, mentioned by Milgrom [5], and Sanders [6]. Basically, modified dynamics is a special rule for doing calculations, and it adds one new basic parameter (which is related to how things speed up or slow down). This means that MOND can determine the strength of gravity within galaxies by only considering the observable matter, such as stars and gas. The Modified Newtonian Dynamics is used to predict how fast stars and gas spin around in flat, spiral-shaped galaxies, and what it predicts often matches exactly what we actually observe.

The fact that this theory works well is a big problem for the Cold Dark Matter theory. This is because the usual idea of dark matter (that it does not interact with normal matter, especially in galaxies) would not naturally create effects that are so perfectly linked to where the normal matter is. For the cold dark matter idea to explain MOND's success, it would mean that dark matter and normal matter must somehow be connected or affect each other. This contradicts the widely accepted scientific view of dark matter's properties.

The MOND easily explains the Tully-Fisher law, discussed by Pizagno et al. [7]. It is a known fact that there is a strong connection between how much normal matter (like stars and gas) a galaxy has and how fast its outer parts rotate. So, the MOND makes this connection a basic rule of how things work, like a special law for galaxies. This Tully-Fisher relation is a problem for the

dark matter theory. In dark matter theory, the spinning speed at a galaxy's edge is mostly maintained by a huge, invisible cloud of dark matter, which is much bigger than the normal stuff in the center of the galaxy. So, it is a bit strange that this speed is so perfectly connected to the small amount of normal matter. The scientists who believe in dark matter say this connection happens because of how galaxies form, but it is hard to understand how such an exact relation could come from a random process, since every galaxy has its own unique history of formation. Most scientists would not fully accept the theory of modified gravity until these bigger ideas are part of a larger and more complete theory. But, since MOND is good at describing what we see in galaxies, that should make us doubt whether cold dark matter exists, addressed by Milgrom [8].

1.3 Newton's law of gravitation

Every particle of matter in the universe attracts every other particle with a force that is directly proportional to the product of their masses and inversely proportional to the square of the distance between their centers.

Mathematically, this is expressed as,

$$F = \frac{Gm_1m_2}{r^2}, \quad (1.1)$$

where, G is the Gravitational constant, $G = 6.67 \times 10^{-11} Nm^2kg^{-2}$. The force is directed along the straight line connecting the centers of the two masses. Unlike electric or magnetic forces, gravity is always attractive and never repulsive. The law applies to all objects with mass, from tiny particles to planets and stars.

1.4 Galaxy dynamics

Galaxy dynamics is the study of how stars, gas, and dark matter move within galaxies under the influence of gravity, revealing their structure, formation,

and evolution. At the center of a galaxy lies the gravitational potential. The potential generated by the overall mass distribution of the galaxy governs the orbital paths of stars and gas clouds. The galaxy consists of the thin and thick disks. The thin disk is a relatively young, dynamically cold structure where stars and gas orbit close to the galactic plane with ordered, nearly circular motions. It contains most of the galaxy's ongoing star formation, along with younger metal-rich stars and interstellar material that gives rise to prominent spiral arms. On the other hand, the thick disk consists of older, dynamically hotter stars that exhibit more random, elongated orbits with greater vertical motions, extending farther above and below the galactic plane. The galactic bars are responsible for the redistribution of angular momentum and the inward transport of gas, which fuels the supermassive black holes residing at the galactic centers. In spiral galaxies like the Milky Way, most stars follow nearly circular orbits within a rotating disk, while in elliptical galaxies, stars move in more random, elongated orbits with higher velocity dispersion.

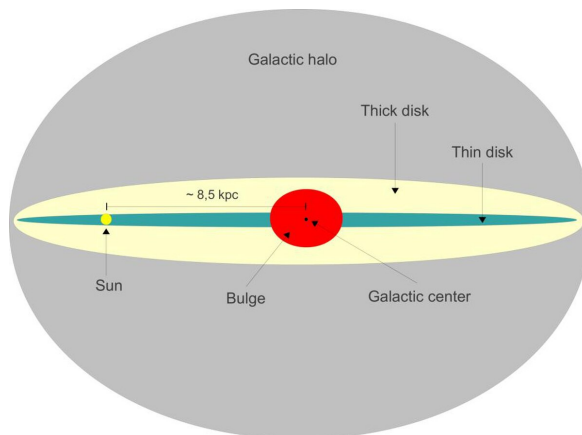


Figure 1.1: Structure of galaxy

Source: <https://shorturl1.at/cFQ4v>

1.5 Rotation curve

The rotation curve of a galaxy is a fundamental observational tool that plots the orbital velocities of stars, gas, and other matter as a function of their dis-

tance from the galactic center. Unlike what Newtonian mechanics predicts for a simple Keplerian system (where most mass is concentrated at the center), galactic rotation curves exhibit surprising behavior that has implications for our understanding of galaxy structure, dark matter, and cosmic evolution examined by Blok et al. [9].

If a galaxy's mass is concentrated in its visible core (like the sun dominates the solar system), orbital speeds obey the Kepler's law as,

$$v(r) = \frac{\sqrt{GM(r)}}{r}, \quad (1.2)$$

where $M(r)$ is the mass enclosed within radius r .

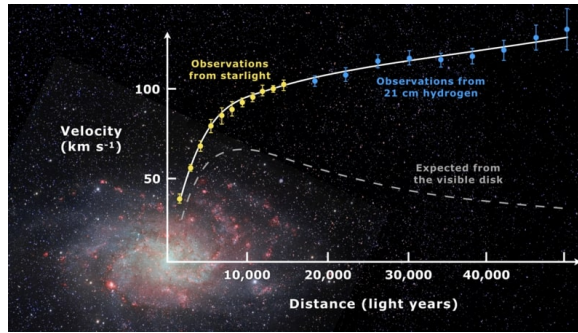


Figure 1.2: Rotation curve of galaxy

Source: <https://shorturl1.at/f031x>

1.6 Scaleheight

The scale height is a fundamental parameter that describes the vertical structure of disk galaxies, quantifying how quickly the density of stars or gas decreases as one moves away from the galactic plane. It is the distance above or below the mid-plane of the disc at which the density of the material (stars, gas) drops to about $1/e$ (roughly 37%) of its value at the mid-plane.

Mathematically, scale height can be expressed as,

$$\rho(z) = \rho_0 e^{-|z|/h}, \quad (1.3)$$

where ρ_0 is a mid-plane density.

A galaxy's vertical exponential material distribution is crucial for its 3-D struc-

ture and dynamics, which arise from an equilibrium between inward gravity and outward kinetic energy (velocity dispersion). The scale height quantifies this distribution, reflecting how galactic forces shape it, and differs by component: e.g., the thin disc (young stars, gas) has a smaller scale height than the older, thick disc.

1.7 Dark matter halo

Dark matter halos are massive, invisible structures that envelop galaxies and galaxy clusters, dominating their gravitational dynamics. Unlike baryonic matter (stars, gas, and dust), dark matter does not emit, absorb, or reflect light, making it detectable only through its gravitational effects. These halos provide the framework for galaxy formation and govern the large-scale structure of the universe.

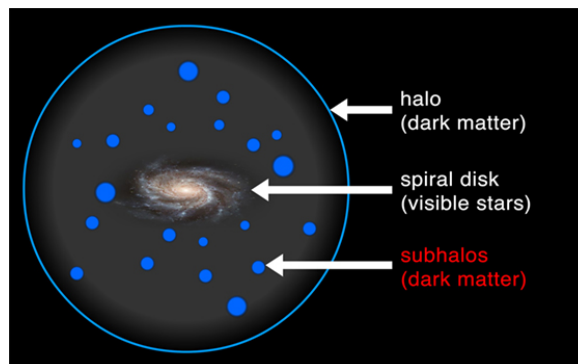


Figure 1.3: Dark matter halo

Source: <https://shorturl.at/c3M6E>

1.8 Interstellar medium

The interstellar medium (ISM) is the matter and radiation that exists in the space between stars within a galaxy. It comprises gas, dust, cosmic rays, and magnetic fields and plays a fundamental role in star formation, galactic evolution, and the recycling of matter in the universe. It is a dynamic, multiphase

environment where physical conditions vary dramatically over scales ranging from sub-parsecs to kilo-parsecs.

1.9 Half-width at half maximum

The Half Width at Half Maximum (HWHM) is a measure of the width of a distribution at half of its maximum amplitude. For a symmetric peak (Gaussian or Lorentzian), the HWHM is simply half of the Full Width at Half Maximum (FWHM). The HWHM of the vertical density profile determines the scale height of the gas layer, helping to understand the hydrostatic balance. If a galaxy's surface brightness follows the Gaussian profile, the HWHM helps determine the scale height of the disk, with larger HWHM values corresponding to more extended structures.

If a distribution $f(x)$ has a maximum value f_{\max} , the HWHM is the distance Δx from the peak center to the point where $f(x) = \frac{f_{\max}}{2}$.

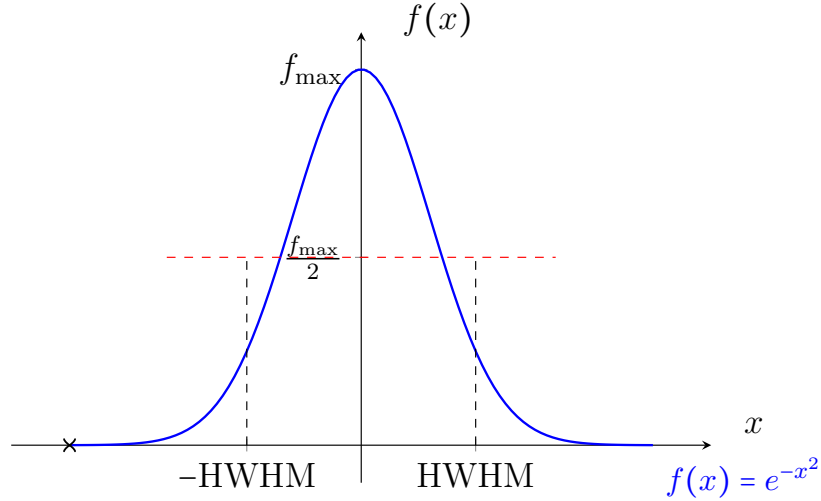


Figure 1.4: Half-width at half maximum

Chapter 2

Galaxy Structure

The galaxies are complex ecosystems that are structured around a central bulge, often spheroidal, dominated by older, dynamically hot stellar populations moving on largely random orbits, and hosting a supermassive black hole whose influence extends throughout the bulge region. The core is embedded within a significantly flattened, rotationally supported galactic disk which is the primary site of baryonic matter, and it comprises the interstellar gas and dust alongside distinct stellar components such as the dynamically cold thin disk rich in young, metal-rich stars, and a vertically thicker, older disk population with higher velocity dispersions. The entire structure is enclosed by a vast, approximately spherical halo, containing a smaller population of ancient stars and globular clusters but dominated dynamically by non-luminous dark matter. The dark matter's gravitational potential determines the mass profile of the galaxy and explains the observed flat rotation curves at large radii. The interplay between these components, which is governed by gravity, hydrodynamics, star formation feedback, and evolutionary processes like mergers, gives information about the observable structure and the ongoing evolution of the galaxy.

2.1 Radial structure

The radial structure of a galaxy describes how its various components, such as stars, gas, dust, and dark matter, are distributed as a function of distance from the galactic center. This structure is governed by gravitational dynamics, angular momentum, and evolutionary processes like star formation.

Galactic Nucleus, Bulge and Disk - The galactic center contains a dense bulge (1 – 3 kpc) of older, metal-rich stars of random orbits, with little recent star formation, and the nucleus often contains a supermassive black hole. The stars follow a Keplerian orbit near the black holes and vary as $v \propto r^{-1/2}$. The galactic bulge varies from 100 pc to 2 kpc. The thin disk is dominated by young stars and gas, whereas the thick disk contains older and metal-poor stars. The surface brightness profile is given as,

$$I(R) = I_0 e^{-R/h_R}, \quad (2.1)$$

where I_0 is the central brightness and h_R is the scale length.

Radial Mass Distribution - The central bulge dominates the mass within the inner 1–2 kpc. Further out, the disk typically contains the majority of the baryonic mass up to 15 kpc. At larger radii (beyond 15 – 20 kpc), the dark matter halo becomes the dominant mass component. Therefore, the outer regions have a higher ratio of mass to light. This is because the star formation slows down further out, and the influence of the dark matter increases.

Radial Gas Distribution - The radial structure of interstellar gas in galactic disks is a bit different. The atomic hydrogen (HI) exhibits the surface density maximum at radii (10–15 kpc) and reaches far beyond the stellar disk (up to 30–50 kpc), indicating high vertical flaring at large radii. The scale height of HI increases with radius due to weaker gravity. On the other hand, the molecular hydrogen (H_2) is more concentrated in the center, and its surface density is highest in the inner disk (3–5 kpc) and decreases sharply with increasing radius. This is due to the fact that the gravitational force in the galaxy decreases as we go further toward the center.

Stellar Surface Density - The stellar surface density Σ_R in galactic disks typically exhibits an exponential decline with radius R , which is given as,

$$\Sigma_R = \Sigma_0 e^{-R/R_d}, \quad (2.2)$$

where Σ_0 is the central surface density and Σ_R is the radial scale length (~ 2.5 – 4 kpc for the Milky Way galaxy).

2.2 Vertical structure

The vertical structure describes how different components of the galaxy are distributed perpendicular to the galactic plane ($z = 0$). This structure arises from the balance between gravitational forces pulling the matter towards the mid-plane and the random motions (kinetic energy) pushing it outward.

Gas Layers - The interstellar medium in the galactic disk has a separation between the vertical gas phase and temperature. The dense part, i.e., the molecular hydrogen, is highly concentrated near the mid-plane with a scale height of ~ 50 – 100 pc and is an active star-forming region. Then there comes a broad layer of neutral atomic hydrogen with a scale height of ~ 200 – 400 pc. Lastly, there is an extremely hot but very low-density coronal gas, which is energized by explosions and extends significantly to the galactic halo, reaching distances of tens of kiloparsecs.

Thin and Thick Disks - For a thin disk, the vertical structure is balanced by the vertical Jeans equation, which is given as,

$$\frac{1}{\rho} \frac{d}{dz} (\rho \sigma_z^2) + \frac{dz}{d\Phi} = 0, \quad (2.3)$$

where σ_z^2 is the vertical velocity dispersion. The thin disk typically consists of stars that are young to intermediate in age (≤ 5 Gyr), which are dynamically cold and have a scale height of ~ 300 – 400 pc. The density profile varies exponentially as $\rho(z) = \rho_0 e^{-|z|/h_z}$. Whereas, the thick disk consists of dynamically hot, older stars ($8 > \text{Gyr}$) and their scale height varies as $h_z \approx 1$ – 1.5 kpc.

Vertical Velocity Dispersion - The vertical scale height of a gas or

stellar component in the galactic disk is associated with its vertical velocity dispersion. The galactic components that have greater vertical velocity dispersion have higher kinetic energy perpendicular to the disk plane, which allows them to occupy larger distances from the mid-plane as opposed to the gravitational potential provided by the disk's total surface mass density. Therefore, dynamically warmer populations like older stars or those making up the thick disk have much larger scale heights. The interstellar gas in galaxies usually moves at relatively low speeds (around 6 – 10 km/s) because of which it tends to stay close to the center of the galaxy, forming a thin compact layer.

2.3 Hydrostatic equilibrium

Hydrostatic equilibrium is a fundamental concept in galactic structure, which describes the balance between two opposing forces in celestial bodies, i.e., gravitational forces pulling matter inward and pressure forces pushing outward. The equilibrium governs the vertical structure of galactic disks and the stability of gas layers, preventing collapse under gravity into space.

In vertical hydrostatic equilibrium, for a gas element at height z in the galactic disk, the equation is given as,

$$\frac{dP}{dz} = -\rho \frac{d\Phi}{dz}, \quad (2.4)$$

where ρ is the mass density, and Φ is gravitational potential. In vertical equilibrium, the scale height for the thin disk is given as $h_z \approx 300$ pc (for $\sigma_z \approx 20$ km/s), and for the thick disk $h_z \approx 1$ kpc (for $\sigma_z \approx 40$ km/s).

In radial equilibrium, in the plane of the disk, the equilibrium is maintained by rotational support, which is given as,

$$v_c^2 = R \frac{dR}{d\Phi}, \quad (2.5)$$

where $v_c(R)$ is the circular velocity. The pressure gradient for the gas disk is given as,

$$\frac{v_c^2}{R} = \frac{1}{\rho} \frac{dP}{dR} + \frac{d\Phi}{dR}. \quad (2.6)$$

In galaxy clusters, hot gas remains bound as the gravitational pull from the cluster's dark matter and galaxies counteracts its thermal pressure. The disturbance in the hydrostatic equilibrium leads to dynamic evolution, so it is a key mechanism in governing the stability and morphology of the galactic structures.

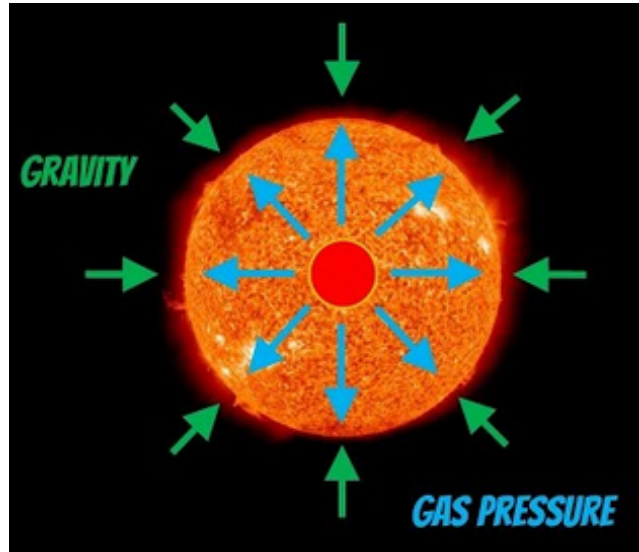


Figure 2.1: Hydrostatic equilibrium

Source: <https://shorturl.at/tYDNk>

Chapter 3

Formulation of Model

The long-observed constancy of the atomic hydrogen (HI) vertical scale height in the inner Galaxy (< 8.5 kpc) discussed by Oort [10], and Dickey [11], contradicts the standard models, which consider only the stellar disk’s gravity, and predict an exponentially increasing scale height with radius. This discrepancy arises because the scale height represents an equilibrium between gravitational force and gas pressure, and as the stellar disk’s pull weakens outwards, the scale height should increase. We argue that accurate modeling of the vertical structure of galactic disks requires including the self-gravity of the gas components (HI and H_2) in addition to that of the stars.

While HI is more dominant in the outer Galaxy where stellar gravity is weak, the significant concentration of molecular hydrogen (H_2) in a ring within the inner Galaxy ($4 - 8.5$ kpc) is proposed to be a key factor. Although gas constitutes only $\sim 15\%$ of the disk surface density, H_2 exists in dense, self-gravitating structures and forms a thin, dynamically influential layer. We present a novel approach by treating stars, HI, and H_2 as three gravitationally coupled components and calculate their scale heights under their joint potential, aiming to explain the observed vertical distributions, including the puzzling constant HI scale heights in the inner disk.

3.1 Assumptions of hydrostatic equilibrium

We model the HI and H_2 gas as thin, axisymmetric, coplanar disks embedded within the stellar disk ($R = 2 - 12$ kpc). Due to the assumed axisymmetry and the thinness of the disk, we neglect gravitational effects in the azimuthal and radial directions, respectively. Therefore, we focus solely on how the mutual gravity modifies the steady-state density distribution along the vertical (z) axis.

The hydrostatic relation between the pull of gravity and the pressure force acting on gas is given by,

$$\langle (v_z)_i^2 \rangle > \frac{\partial \rho_i}{\partial z} = -\rho_i \frac{\partial \psi}{\partial z}, \quad (3.1)$$

where, $\langle (v_z)_i^2 \rangle$ is the root mean square of vertical velocities in z - direction, ψ is the gravitational potential, and $i = s, \text{ HI}, H_2$ denotes the quantities for stars, HI, H_2 respectively.

3.2 Establishment of the equation

The force equation along the z -axis using the equation (3.1) and considering all the disc components is given by,

$$\frac{\langle (v_z)_i^2 \rangle}{\rho_i} \frac{d\rho_i}{dz} = \left(\frac{-d\psi}{dz} \right)_s + \left(\frac{-d\psi}{dz} \right)_{HI} + \left(\frac{-d\psi}{dz} \right)_{H_2} + \left(\frac{-d\psi}{dz} \right)_{DM}, \quad (3.2)$$

where $\left(\frac{-\partial \psi}{\partial z} \right)$ is the force per unit mass along the z -axis. The last term denotes the force along the z -axis due to the dark matter halo. The thin disk's vertical influence on the halo is neglected. The component is assumed vertically isothermal, using its vertical velocity dispersion $\langle (v_z)_i^2 \rangle$. The entire right side of the equation (3.2) is the total vertical force from all components. The Poisson equation is given as,

$$\nabla^2 \psi = 4\pi G \rho. \quad (3.3)$$

For a thin axisymmetric disk and gravitationally coupled system, the joint Poisson equation reduces to,

$$\frac{d^2\psi_S}{dz^2} + \frac{d^2\psi_{HI}}{dz^2} + \frac{d^2\psi_{H_2}}{dz^2} = 4\pi G(\rho_S + \rho_{HI} + \rho_{H_2}). \quad (3.4)$$

Differentiating equation (3.2) with respect to z ,

$$\frac{\langle (v_z)_i^2 \rangle}{\rho_i} \frac{d^2\rho_i(z)}{dz^2} - \left(\frac{d\rho_i(z)}{dz} \right)^2 \frac{\langle (v_z)_i^2 \rangle}{\rho_i^2} = - \left[\frac{d^2\psi_S}{dz^2} + \frac{d^2\psi_{HI}}{dz^2} + \frac{d^2\psi_{H_2}}{dz^2} \right] - \frac{d^2\psi_{DM}}{dz^2}. \quad (3.5)$$

Using equation (3.4) in equation (3.5), we get,

$$\frac{\langle (v_z)_i^2 \rangle}{\rho_i} \frac{d^2\rho_i(z)}{dz^2} = - \left[4\pi G(\rho_S + \rho_{HI} + \rho_{H_2}) + \frac{d^2\psi_{DM}}{dz^2} \right] + \frac{\langle (v_z)_i^2 \rangle}{\rho_i^2} \left(\frac{d\rho_i(z)}{dz} \right)^2, \quad (3.6)$$

$$\implies \frac{d^2\rho_i}{dz^2} = \frac{\rho_i}{\langle (v_z)_i^2 \rangle} \left[-4\pi G(\rho_S + \rho_{HI} + \rho_{H_2}) - \frac{d^2\psi_{DM}}{dz^2} \right] + \frac{1}{\rho_i} \left(\frac{d\rho_i}{dz} \right)^2. \quad (3.7)$$

The terms contained in the square brackets of equation (3.7) arise due to the joint potential of the three disk components (for i = stars, HI, and H_2). The vertical velocity dispersion varies with each component despite having a common gravitational potential.

3.3 Methods for solving equations

3.3.1 Solution of equations

The equation (3.7) can be split into a system of first-order ODEs for the sake of simplicity. We will solve them numerically using the fourth-order Runge-Kutta method. The required initial conditions at mid-plane, $z = 0$, for each component i are derived from the physical boundary conditions:

$$\rho_i = (\rho_0)_i \quad \text{and} \quad \frac{d\rho_i}{dz} = 0. \quad (3.8)$$

By assuming the vertical homogeneity near the mid-plane, we get information about the boundary condition for each component i , where i varies for stars, HI, and H_2 . In this formulation, the mid-plane density is not specified a priori but becomes an outcome determined by the constraint that the vertically inte-

grated density profile must dictate the known surface density at the considered radius R , treating the vertical structure as a one-dimensional problem.

The coupled density distributions for stars (ρ_s), atomic hydrogen (ρ_{HI}), and molecular hydrogen H_2 (ρ_{H_2}) at a given radius R are solved simultaneously using an iterative scheme via equation (3.7). Initially, $\rho_s(z)$ is calculated neglecting gas contributions, then $\rho_{HI}(z)$ is calculated using $\rho_s(z)$, neglecting $\rho_{H_2}(z)$, and finally $\rho_{H_2}(z)$ is determined using the derived $\rho_s(z)$ and $\rho_{HI}(z)$. To account for the coupling, ρ_s is re-evaluated incorporating the computed gas densities, and this full cycle is repeated four times until all distributions converge to within fifth decimal accuracy, reflecting their mutual gravitational influence.

3.3.2 Parameters used

For each component, i.e., stars, HI, and H_2 at radius R , the surface density and vertical velocity dispersion must be specified. All the gas parameters and the stellar velocity dispersion are taken from observations by Scoville et al. [12]. The stellar surface density is taken from the literature discussed in Sanders et al. [13]. The stellar disk surface density distribution is determined by two key parameters, which are the local stellar surface density and the exponential radial scale length (h_R).

We adopt the Mera et al. [14] model as our standard galactic mass framework because it offers a modern and simple structure suitable for analyzing component effects, employs plausible parameters which are consistent with accepted ranges, ensuring internal consistency by drawing parameters from a single source, and incorporates a screened halo profile which is sufficient for capturing the halo's dynamical influence suggested by Narayan and Jog [15].

3.4 Mathematical formulation

The Laplacian in spherical coordinates is expressed as,

$$\nabla^2\psi = \frac{1}{r^2} \frac{\partial}{\partial r} \left(r^2 \frac{\partial\psi}{\partial r} \right) + \frac{1}{r^2 \sin\theta} \frac{\partial}{\partial\theta} \left(\sin\theta \frac{\partial\psi}{\partial\theta} \right) + \frac{1}{r^2 \sin^2\theta} \frac{\partial^2\psi}{\partial\phi^2}. \quad (3.9)$$

From equation (3.9), the radial component is given by the term,

$$\frac{1}{r^2} \frac{d}{dr} \left(r^2 \frac{d\psi}{dr} \right).$$

From equation (3.3),

$$\nabla^2\psi = 4\pi G\rho(r) = \frac{1}{r^2} \frac{d}{dr} \left(r^2 \frac{d\psi}{dr} \right). \quad (3.10)$$

Gravitational potential is related to v_{rot} as,

$$v_{rot}^2 = r \frac{d\psi}{dr}. \quad (3.11)$$

In spherical coordinates, the density profile for the halo is given by,

$$\rho_{DM}(r) = \frac{v_{rot}^2}{4\pi G} \frac{1}{R_c^2 + r^2}. \quad (3.12)$$

where ρ_{DM} is the dark matter halo mass density, R_c is the core radius = 5 kpc and v_{rot} is the circular velocity = 220 km/s.

From equations (3.10) and (3.12) we get,

$$\frac{1}{r^2} \frac{d}{dr} \left(r^2 \frac{d\psi}{dr} \right) = \frac{v_{rot}^2}{R_c^2 + r^2}. \quad (3.13)$$

Integrating with respect to r ,

$$\begin{aligned} \int \frac{d}{dr} \left(r^2 \frac{d\psi}{dr} \right) dr &= v_{rot}^2 \int \frac{r^2}{R_c^2 + r^2} dr, \\ \implies r^2 \frac{d\psi}{dr} &= v_{rot}^2 \int \frac{r^2}{R_c^2 + r^2} dr, \\ \implies r^2 \frac{d\psi}{dr} &= v_{rot}^2 \int \left(1 - \frac{R_c^2}{R_c^2 + r^2} \right) dr, \\ \implies r^2 \frac{d\psi}{dr} &= v_{rot}^2 \int \left[r - \int \frac{R_c^2}{R_c^2 + r^2} \right] dr, \\ \implies r^2 \frac{d\psi}{dr} &= v_{rot}^2 \left[r - \int \frac{dr}{1 + \left(\frac{r}{R_c} \right)^2} \right], \end{aligned} \quad (3.14)$$

$$\begin{aligned}
&\implies r^2 \frac{d\psi}{dr} = v_{rot}^2 \left[r - \tan^{-1} \left(\frac{r}{R_c} \right) \right], \\
&\implies \frac{d\psi}{dr} = v_{rot}^2 \left[\frac{1}{r} - \frac{1}{r^2} \tan^{-1} \left(\frac{r}{R_c} \right) \right]. \tag{3.15}
\end{aligned}$$

Again, integrating equation (3.15) with respect to r ,

$$\psi_{DM}(r) = v_{rot}^2 \left[\frac{dr}{r} - \frac{1}{r^2} \tan^{-1} \left(\frac{r}{R_c} \right) dr \right], \tag{3.16}$$

$$\begin{aligned}
&\implies \psi_{DM}(r) = v_{rot}^2 \left[\log r - \left[\tan^{-1} \left(\frac{r}{R_c} \right) \left(\frac{-1}{r} \right) - \int \frac{R_c^2}{R_c^2 + r^2} \left(\frac{-1}{r} \right) \right] \right], \\
&\implies \psi_{DM}(r) = v_{rot}^2 \left[\log r + \frac{1}{r} \tan^{-1} \left(\frac{r}{R_c} \right) - \int \frac{R_c^2}{r^3 \left(1 + \left(\frac{R_c}{r} \right)^2 \right)} dr \right]. \tag{3.17}
\end{aligned}$$

Assume,

$$I = \int \frac{R_c^2}{r^3 \left(1 + \left(\frac{R_c}{r} \right)^2 \right)} dr.$$

$$\text{Let, } t = 1 + \frac{R_c^2}{r^2}, \implies \frac{dt}{-2} = \frac{R_c^2}{r^3} dr.$$

So,

$$\begin{aligned}
I &= -\frac{1}{2} \int \frac{dt}{t} = -\frac{1}{2} \ln t, \\
I &= -\frac{1}{2} \log(r^2 + R_c^2) + \log(r).
\end{aligned}$$

By using the above value of I in equation (3.17), we get $\psi_{DM}(r)$ as,

$$\psi_{DM}(r) = v_{rot}^2 \left[1 - \frac{1}{2} \log(R_c^2 + r^2) - \frac{R_c}{r} \tan^{-1} \left(\frac{r}{R_c} \right) \right]. \tag{3.18}$$

In cylindrical coordinate system, we have the relation between R , r , and z as,

$$r = \sqrt{R^2 + z^2}. \tag{3.19}$$

So, rewriting the equation (3.18) using equation (3.19),

$$\psi_{DM}(r) = v_{rot}^2 \left[1 - \frac{1}{2} \log(R_c^2 + R^2 + z^2) - \frac{R_c}{\sqrt{R^2 + z^2}} \tan^{-1} \left(\frac{\sqrt{R^2 + z^2}}{R_c} \right) \right]. \tag{3.20}$$

Taking the first derivative of ψ with respect to z ,

$$\frac{d\psi_{DM}}{dz} = v_{rot}^2 \left[\frac{-z}{R_c^2 + R^2 + r^2} + \frac{zR_c}{(R^2 + z^2)^{3/2}} \tan^{-1} \left(\frac{\sqrt{R^2 + z^2}}{R_c} \right) - \frac{zR_c^2}{(R^2 + z^2)(R_c^2 + R^2 + r^2)} \right]. \quad (3.21)$$

Again, taking the derivative of the above equation with respect to z and rearranging the terms,

$$\begin{aligned} \frac{\partial^2 \psi_{DM}}{\partial z^2} = & \frac{v_{rot}^2 R_c}{(R^2 + z^2)^{3/2}} \tan^{-1} \left(\frac{\sqrt{R^2 + z^2}}{R_c} \right) \left[1 - \frac{3z^2}{R^2 + z^2} \right] + \\ & \frac{z^2 R_c^2 v_{rot}^2}{(R^2 + z^2)^2 (R_c^2 + R^2 + z^2)} + \frac{v_{rot}^2}{(R^2 + z^2)} \left[\frac{2z^2}{R^2 + z^2} - 1 \right]. \end{aligned} \quad (3.22)$$

3.5 Observations

The observations are made by using the galactic mass model of Mera et al. [14] for the vertical scale height as a function of galactic radius.

- a.** The effect of the different components of the galaxy is seen in different galactocentric radii. The stars dominate in the inner few kpc, determining the scale height in this region. The effect of H_2 is seen in the region between 4–8.5 kpc, while the impact of HI is seen beyond 8.5 kpc. This happens because the inner part of the galaxy is dominated by the stars and H_2 , and HI becomes dominant only in the outer region.
- b.** The inclusion of dark matter halo potential into the calculation leads to a reduction in the HI scale height. This is contrary to the general expectation of the literature, and this happens because the dark matter and baryonic matter dominate in different ranges of z . In a self-gravitating disk, more than 99% of its baryonic matter is concentrated within $z \leq 1$ kpc, confining the influence of baryonic matter in this region.
- c.** The vertical support of HI comes only from the turbulent gas pressure derived from its vertical velocity dispersion, without considering the magnetic pressure. This approach is chosen for simplicity, and it matches with the argument of Lockman et al. [16] for their three-component system.

Chapter 4

Formulation of MOND

4.1 Introduction

Sanders and McGaugh [17] tested the Modified Newtonian Dynamics (MOND) using the observed flaring of the Milky Way’s neutral hydrogen (HI) gas layer, assuming hydrostatic equilibrium. We developed a framework to predict the HI scale height in MOND, and the results show that MOND provides a good fit to the observed flaring beyond 17 kpc using a constant gas velocity dispersion (≈ 9 km/s), but significantly underpredicts the scale height between 10–16 kpc compared to observations. Despite this discrepancy, considering uncertainties (e.g., non-thermal pressures) addressed by Olling [18], and Combes [19], we presented MOND as a plausible alternative to dark matter for explaining the flaring and we study HI flaring in external galaxies as a promising method to further test MOND’s viability and build upon its known success in reproducing galaxy rotation curves without dark matter.

The Milky Way provides an excellent test case for gravity theories due to its well-characterized structure and observed HI flaring observed by Kalberla et al. [20]. The standard Newtonian model or CDM models struggle to explain this flaring, requiring complex dark matter distributions that contradict other halo shape estimates and standard CDM expectations, possibly indicating incomplete modeling. Since MOND is often considered more constrained

(because of fewer free parameters), this study investigates whether it can successfully explain the galactic flaring solely using the observed baryonic matter distribution, posing a potentially more rigorous test mentioned by Sanchez et al. [21].

4.2 Mathematical framework

4.2.1 Assumption of the modified Poisson equation

In the modified Newtonian dynamics theory, the Poisson equation is modified to account for the behavior of gravity in regimes of very low acceleration. The goal of MOND is to explain the observed dynamics of galaxies without invoking dark matter. In order to derive the modified Poisson equation in MOND, we start with the standard Poisson equation and then introduce the modifications specific to MOND.

In Newtonian gravity, the Poisson equation is given by,

$$\nabla^2\Phi = 4\pi G\rho, \quad (4.1)$$

where Φ is the gravitational potential, ρ is the mass density, and G is the gravitational constant.

MOND modifies the Newtonian dynamics at low accelerations (much less than a characteristic acceleration a_0). So, instead of using Newton's second law $F = ma$, MOND suggests,

$$\mu\left(\frac{|\mathbf{g}|}{a_0}\right)\mathbf{g} = -\nabla\Phi, \quad (4.2)$$

where \mathbf{g} is the gravitational field, a_0 is a fundamental acceleration scale in MOND ($\approx 1.2 \times 10^{-10} m s^{-2}$), and $\mu(x)$ is an interpolation function.

For large accelerations ($|\mathbf{g}| \gg a_0$), $\mu(x) \approx 1$, we recover Newtonian gravity and for low accelerations ($|\mathbf{g}| \ll a_0$), $\mu(x) \approx x$, leads to MONDian acceleration.

To derive the modified Poisson equation, we need the relation between the gravitational field \mathbf{g} and the potential, which is given as,

$$\mathbf{g} = -\nabla\Phi. \quad (4.3)$$

From equation (4.2),

$$\mu \left(\frac{|\mathbf{g}|}{a_0} \right) \mathbf{g} = -\nabla \Phi. \quad (4.4)$$

Taking the divergence on both sides,

$$\nabla \cdot \left[\mu \left(\frac{|\mathbf{g}|}{a_0} \right) \mathbf{g} \right] = \nabla \cdot (-\nabla \Phi), \quad (4.5)$$

$$\implies \nabla \cdot \left[\mu \left(\frac{|\mathbf{g}|}{a_0} \right) \mathbf{g} \right] = -\nabla^2 \Phi. \quad (4.6)$$

Substituting equations (4.1) and (4.2) into equation (4.6),

$$\nabla \cdot \left[\mu \left(\frac{|\nabla \Phi|}{a_0} \right) (-\nabla \Phi) \right] = -4\pi G \rho. \quad (4.7)$$

Upon simplifying,

$$\nabla \cdot \left[\mu \left(\frac{|\nabla \Phi|}{a_0} \right) \nabla \Phi \right] = 4\pi G \rho. \quad (4.8)$$

This is the modified Poisson equation in modified dynamics. It differs from the standard Poisson equation in that the Laplacian operator ∇^2 is replaced by a more complex operator involving the function μ , which depends on the magnitude of the gravitational field $|\nabla \Phi|$.

The function $\mu(x)$ interpolates between the Newtonian regime (where $\mu \approx 1$) and the deep MOND regime (where $\mu(x) \approx x$). The exact form of $\mu(x)$ can vary depending on the specific version of MOND, but a common choice is $\mu(x) = x/(1+x^2)^{1/2}$ Bekenstein [22].

4.2.2 Expression for fictitious dark matter

The Poisson equation as given by equation (4.1) is,

$$\nabla^2 \Phi = 4\pi G \rho_{tot}, \quad (4.9)$$

where ρ_{tot} is the total mass density, which includes both baryonic matter ρ and dark matter ρ_{dm} . So, $\rho_{tot} = \rho + \rho_{dm}$.

Then equation (4.9) becomes,

$$\nabla^2 \Phi = 4\pi G (\rho + \rho_{dm}). \quad (4.10)$$

ρ_{dm} can be calculated as,

$$\rho_{dm} = (4\pi G)^{-1} \nabla^2 \Phi - \rho. \quad (4.11)$$

4.2.3 Expression for surface density of fictitious dark matter

Consider an isothermal, self-gravitating layer of baryons with surface density Σ_b . The Newtonian acceleration g_N at the surface is related to the baryonic surface density Σ_b as,

$$g_N = 2\pi G \Sigma_b^N. \quad (4.12)$$

$$\implies \Sigma_b^N = \frac{g_N}{2\pi G}. \quad (4.13)$$

Now, the contribution of dark matter to the gravitational force can be expressed as,

$$\Sigma_{dm} = \frac{g_{dm}}{2\pi G}. \quad (4.14)$$

So, the total effective gravitational force can be expressed as the sum of baryonic matter and dark matter contributions, which is given as,

$$g = g_N + g_{dm}. \quad (4.15)$$

$$g = 2\pi G \Sigma_b + 2\pi G \Sigma_{dm}. \quad (4.16)$$

The Newtonian gravity or acceleration is related to MONDian acceleration by the relation as,

$$g_N = g\mu. \quad (4.17)$$

$$g = \frac{g_N}{\mu}. \quad (4.18)$$

Using equation (4.12), we get,

$$g = \frac{2\pi G \Sigma_b}{\mu}. \quad (4.19)$$

From equation (4.16) we have,

$$2\pi G \Sigma_{dm} = g - 2\pi G \Sigma_b. \quad (4.20)$$

Using equation (4.19) in equation (4.20),

$$2\pi G \Sigma_{dm} = \frac{2\pi G \Sigma_b}{\mu} - 2\pi G \Sigma_b, \quad (4.21)$$

$$\implies \Sigma_{dm} = \left[\frac{1}{\mu(g/a_0)} - 1 \right] \Sigma_b, \quad (4.22)$$

where Σ is the real (baryonic) surface density of the disc and g is the total MOND acceleration just outside the disc, Milgrom [23].

4.2.4 Scale height of 1-D planar mass layer

Assuming the pure planar symmetry, we take into consideration the equation of vertical hydrostatic equilibrium, which consists of the two opposing forces: the gravitational force and the pressure gradient.

The gravitational force per unit volume acting on a small element of mass at height z above the mid-plane is given as $-\rho \frac{d\Phi}{dz}$, where ρ is mass density at height z , and $\frac{d\Phi}{dz}$ is the vertical component of the gravitational force.

The pressure gradient force per unit volume, which resists the gravitational force, is given as $-\frac{dP}{dz}$.

In the state of vertical hydrostatic equilibrium, the gravitational force is balanced by the pressure gradient as,

$$-\frac{dP}{dz} = -\left(-\rho \frac{d\Phi}{dz}\right), \quad (4.23)$$

$$\implies \frac{dP}{dz} = -\rho \frac{d\Phi}{dz}. \quad (4.24)$$

From equation (4.8),

$$\nabla \cdot \left[\mu \left(\frac{|\nabla \Phi|}{a_0} \right) \nabla \Phi \right] = 4\pi G \rho. \quad (4.25)$$

For one-dimensional system, i.e., z -axis, the gradient operator will be written as,

$$\left(\frac{d}{dz} \left[\mu \left(\frac{d\Phi}{a_0 dz} \right) \frac{d\Phi}{dz} \right] \right) (4\pi G)^{-1} = \rho. \quad (4.26)$$

Integrating the equation (4.24) from 0 to z and use equation (4.26) to replace ρ ,

$$\int_0^z \frac{dP}{dz'} dz' = -(4\pi G)^{-1} \int_0^z \frac{d}{dz'} \left(\mu \frac{d\Phi(z')}{a_0 dz'} \right) \frac{d\Phi(z')}{dz'} dz'. \quad (4.27)$$

In deep MOND, we have the relation as,

$$\mu \approx \frac{d\Phi(z)}{dz} \frac{1}{a_0} \approx \mu \frac{d\Phi(z)}{a \cdot dz}.$$

Using the above relation in equation (4.27),

$$P(z) - P(0) = -\frac{(4\pi G)^{-1}}{a_0} \int_0^z \frac{d}{dz'} \left(\frac{d\Phi(z')}{dz'} \frac{d\Phi(z')}{dz'} \right) \frac{d\Phi(z')}{dz'} dz', \quad (4.28)$$

$$P(z) - P(0) = -\frac{(4\pi G)^{-1}}{a_0} \int_0^z \frac{d}{dz'} \left(\frac{d\Phi(z')}{dz'} \right)^2 \frac{d\Phi(z')}{dz'} dz',$$

$$P(z) - P(0) = -\frac{1}{4\pi G a_0} \int_0^z 2 \frac{d\Phi(z')}{dz'} \frac{d^2\Phi(z')}{dz'^2} \frac{d\Phi(z')}{dz'} dz',$$

$$P(z) - P(0) = -\frac{2}{4\pi G a_0} \int_0^z \left(\frac{d\Phi(z')}{dz'} \right)^2 \frac{d^2\Phi(z')}{dz'^2} dz'. \quad (4.29)$$

Let

$$dv = \frac{d^2\Phi(z')}{dz'^2} dz', \implies v = \frac{d\Phi(z')}{dz'^2},$$

and,

$$u = \left(\frac{d\Phi(z')}{dz'} \right)^2.$$

Now, using integration by parts,

$$P(z) - P(0) = -\frac{1}{2\pi G a_0} \left[\left(\frac{d\Phi(z')}{dz'} \right)^2 \left(\frac{d\Phi(z')}{dz'} \right) \right]_0^z - 2 \int_0^z \frac{d\Phi(z')}{dz'} \cdot \frac{d^2\Phi(z')}{dz'^2} \cdot \frac{d\Phi(z')}{dz'} dz', \quad (4.30)$$

$$P(z) - P(0) = -\frac{1}{2\pi G a_0} \left[\left(\frac{d\Phi(z')}{dz'} \right)^2 \left(\frac{d\Phi(z')}{dz'} \right) - 0 \right] \frac{1}{3},$$

$$P(z) - P(0) = -\frac{1}{6\pi G a_0} \left(\frac{d\Phi(z')}{dz'} \right)^3. \quad (4.31)$$

Now, integrate equation (4.8) from $-z$ to z ,

$$\int_{-z}^z \frac{d}{dz'} \left(\frac{d\Phi}{dz'} \frac{d\Phi}{dz'} \right) dz' = \int_{-z}^z 4\pi G \rho a_0, \quad (4.32)$$

$$\implies \int_{-z}^z \frac{d}{dz'} \left(\frac{d\Phi}{dz'} \right)^2 dz' = 4\pi G a_0 \int_{-z}^z \rho dz',$$

$$\implies 2 \left(\frac{d\Phi(z)}{dz} \right)^2 = 4\pi G a_0 \Sigma(z),$$

where, $\Sigma(z) = \int_{-z}^z \rho dz'$.

$$\implies \frac{d\Phi(z)}{dz} = \sqrt{2\pi G a_0 \Sigma(z)}. \quad (4.33)$$

The right-hand side represents the integrated surface density.

Using equation (4.33) in equation (4.31),

$$P(z) - P(0) = -\frac{1}{6\pi Ga_0}(2\pi Ga_0 \Sigma(z))^{3/2}, \quad (4.34)$$

$$P(z) - P(0) = -\frac{1}{3}(2\pi Ga_0)^{1/2} \Sigma(z)^{3/2}. \quad (4.35)$$

For an isothermal and isotropic gas with 1-D velocity dispersion σ , the mid-plane pressure is $P(0) = \rho_0 \sigma^2$, where ρ_0 is the density at $z = 0$. Considering the boundary conditions $P(\infty) = 0$ we get,

$$\rho_0 \sigma^2 = \frac{1}{3}(2\pi Ga_0)^{1/2} \Sigma(z)^{3/2}. \quad (4.36)$$

The scale height z_0 is defined as,

$$z_0 = \frac{\Sigma_\infty}{2\rho_0}. \quad (4.37)$$

From equation (4.36),

$$2\rho_0 \sigma^2 = \frac{2}{3}(2\pi Ga_0 \Sigma_\infty)^{1/2} \Sigma_\infty, \quad (4.38)$$

$$\implies \frac{\Sigma_\infty}{2\rho_0} = \frac{3\sigma^2}{2\sqrt{2\pi Ga_0 \Sigma_\infty}} = z_0,$$

$$\implies z_0 = \frac{3\sigma^2}{2\sqrt{2\pi Ga_0 \Sigma_\infty}} \cdot \frac{2\pi Ga_0 \Sigma_\infty}{2\pi Ga_0 \Sigma_\infty},$$

$$\implies z_0 = \frac{3\sigma^2 \sqrt{2\pi Ga_0 \Sigma_\infty}}{4\pi Ga_0 \Sigma_\infty}. \quad (4.39)$$

Finally, the scale height in terms of μ can be given as,

$$z_0 = \frac{3\sigma^2 \mu_\infty}{4\pi G \Sigma_\infty}. \quad (4.40)$$

where $\mu_\infty = \frac{\sqrt{2\pi Ga_0 \Sigma_\infty}}{a_0}$, is the relation between μ and Σ .

4.2.5 Gravitational potential in axisymmetric thin discs

The modified Poisson equation is difficult to solve numerically, but it can be simplified by considering the vertical structure of the outer parts of axisymmetric discs. The field equation can be written as,

$$\nabla \mu(x) \cdot \nabla \phi + \mu(x) \nabla^2 \phi = 4\pi G \rho. \quad (4.41)$$

where $x = \frac{|\nabla \phi|}{a_0}$.

In cylindrical coordinates (R, z) , the gradient can be expressed as,

$$\nabla\phi = \frac{\partial\phi}{\partial R}\hat{R} + \frac{1}{R}\frac{\partial\phi}{\partial\phi}\hat{\phi} + \frac{\partial\phi}{\partial z}\hat{z}. \quad (4.42)$$

The Laplacian can be expressed as,

$$\nabla^2\phi = \frac{\partial^2\phi}{\partial R^2} + \frac{1}{R}\frac{\partial\phi}{\partial R} + \frac{\partial^2\phi}{\partial z^2}. \quad (4.43)$$

Now we calculate,

$$\nabla\phi \cdot \nabla\mu(x) = \left(\frac{\partial\phi}{\partial R}\hat{R} + \frac{\partial\phi}{\partial z}\hat{z} \right) \cdot \left(\frac{\partial\mu(x)}{\partial R}\hat{R} + \frac{\partial\mu(x)}{\partial z}\hat{z} \right), \quad (4.44)$$

$$\implies \nabla\phi \cdot \nabla\mu(x) = \frac{\partial\phi}{\partial R} \cdot \frac{\partial\mu}{\partial R} + \frac{\partial\phi}{\partial z} \cdot \frac{\partial\mu}{\partial z}. \quad (4.45)$$

Using equation (4.45) in equation (4.41),

$$\mu(x)\nabla^2\phi + \left(\frac{\partial\phi}{\partial R} \cdot \frac{\partial\mu}{\partial R} + \frac{\partial\phi}{\partial z} \cdot \frac{\partial\mu}{\partial z} \right) = 4\pi G\rho, \quad (4.46)$$

$$\mu(x)\nabla^2\phi + \left(\frac{\partial\phi}{\partial R} \frac{\partial\mu}{\partial R} \right) \left[1 + \left(\frac{\partial\phi}{\partial z} \cdot \frac{\partial\mu}{\partial z} \right) \left(\frac{\partial\phi}{\partial R} \right)^{-1} \left(\frac{\partial\mu}{\partial R} \right)^{-1} \right] = 4\pi G\rho,$$

$$\mu(x)\nabla^2\phi + \left(\frac{\partial\phi}{\partial R} \frac{\partial\mu}{\partial R} \right) \left[1 + \left(\frac{\partial\phi}{\partial z} \right) \left(\frac{\partial\phi}{\partial R} \right)^{-1} \left(\frac{\partial\mu}{\partial z} \right) \left(\frac{\partial\mu}{\partial R} \right)^{-1} \right] = 4\pi G\rho,$$

$$\mu(x)\nabla^2\phi + \left(\frac{\partial\phi}{\partial R} \frac{\partial\mu}{\partial R} \right) [1 + \zeta_\phi(R, z)\zeta_\mu(R, z)] = 4\pi G\rho,$$

$$\mu(x)\nabla^2\phi + \left(\frac{\partial\phi}{\partial R} \frac{\partial\mu}{\partial R} \right) (1 + \zeta) = 4\pi G\rho. \quad (4.47)$$

where $\zeta = \zeta_\phi\zeta_\mu$, with,

$$\zeta_\phi(R, z) = \left(\frac{\partial\phi}{\partial z} \right) \left(\frac{\partial\phi}{\partial R} \right)^{-1} = \frac{g_z}{g_R}, \quad (4.48)$$

and,

$$\zeta_\mu(R, z) = \left(\frac{\partial\mu}{\partial z} \right) \left(\frac{\partial\mu}{\partial R} \right)^{-1} = \left(\frac{\partial g}{\partial z} \right) \left(\frac{\partial g}{\partial R} \right)^{-1}. \quad (4.49)$$

This equation (4.47) is equivalent to the original one for axisymmetric systems.

The factor $\left(\frac{\partial\phi}{\partial R} \frac{\partial\mu}{\partial R} \right)$ in equation (4.47) can be rewritten as,

$$\left(\frac{\partial\phi}{\partial R} \frac{\partial\mu}{\partial R} \right) = \frac{d\mu}{dx} \frac{\partial\phi}{\partial R} \frac{\partial x}{\partial R} \approx \frac{d\mu}{dx} \frac{\partial\phi}{\partial R} \frac{d}{dR} \left(\frac{v_c^2}{R} \right). \quad (4.50)$$

The Laplacian can be written as,

$$\nabla^2 \phi = \frac{1}{R} \frac{\partial}{\partial R} \left(R \frac{\partial \phi}{\partial R} \right) + \frac{\partial^2 \phi}{\partial z^2}, \quad (4.51)$$

$$\implies \nabla^2 \phi = \frac{1}{R} \frac{\partial v_c^2}{\partial R} + \frac{\partial^2 \phi}{\partial z^2}. \quad (4.52)$$

Using equations (4.50) and (4.52) in equation (4.47), we obtain,

$$\frac{\mu}{R} \frac{\partial v_c^2}{\partial R} + \mu \frac{\partial^2 \phi}{\partial z^2} + \left(\frac{d\mu}{dx} \frac{\partial \phi}{\partial R} \frac{\partial}{\partial R} \left(\frac{v_c^2}{R} \right) \right) (1 + \zeta) = 4\pi G \rho, \quad (4.53)$$

$$\frac{\mu}{R} \frac{\partial v_c^2}{\partial R} + \mu \frac{\partial^2 \phi}{\partial z^2} + \left(\frac{d\mu}{dx} \frac{v_c^2}{a_0 R} \frac{d}{dR} \left(\frac{v_c^2}{R} \right) \right) (1 + \zeta) = 4\pi G \rho,$$

$$\mu \frac{\partial^2 \phi}{\partial z^2} = 4\pi G \rho - (1 + \zeta) \frac{v_c^2}{a_0 R} \frac{d\mu}{dx} \frac{d}{dR} \left(\frac{v_c^2}{R} \right) - \frac{\mu}{R} \frac{dv_c^2}{dR},$$

where v_c is the circular velocity at the mid-plane.

$$\frac{\partial^2 \phi}{\partial z^2} = 4\pi \frac{G}{\mu} \rho - (1 + \zeta) L(x) \frac{d}{dR} \left(\frac{v_c^2}{R} \right) - \frac{1}{R} \frac{dv_c^2}{dR}. \quad (4.54)$$

where $L(x) = \frac{d \ln \mu}{d \ln x}$ is the logarithmic derivative and is known as L-term. The vertical distribution for an isothermal disc can be obtained by combining the equations (4.24) and (4.54). The fictitious dark disc and the fictitious round dark disc are predicted by MOND, and the resultant flattened potential along the vertical axis shows that MOND is correct.

Chapter 5

Numerical Implementation and Result

The differential equations described in the previous chapters are not feasible to solve analytically, so in order to compute those equations, we need numerical methods. We adopt a numerical approach to solve them. The methods which are adopted here are the Dormand-Prince 5th order method, the Runge-Kutta 8th order method. While these methods are extensively available within the SciPy package of Python, here we give the mathematical description of these methods.

5.1 DOPRI5

The Dormand-Prince method of 5th order (DOPRI5) is an embedded Runge-Kutta (RK) method designed for solving ordinary differential equations with high accuracy and adaptive step-size control. The embedded RK methods compute two solutions of different orders (e.g., 4th and 5th) using the same function evaluations. The difference between these solutions provides an error estimate, allowing adaptive step-size adjustment. This method provides the 5th order solution, which is the primary high-accuracy result, the 4th order embedded solution for error estimation, and requires 7 function evaluations

per step.

Consider an ordinary differential equation of the form,

$$\frac{dy}{dt} = f(t, y), \quad y(t_0) = y_0. \quad (5.1)$$

The s -stage Runge-Kutta method is computed as,

$$y_{n+1} = y_n + h \sum_{i=1}^s b_i k_i, \quad (5.2)$$

where,

$$k_i = f \left(t_n + c_i h, y_n + h \sum_{j=1}^s a_{ij} k_j \right). \quad (5.3)$$

The values for c_i , a_{ij} , and b_i can be found using the Butcher table as given below.

c_i	a_{ij}	b_i (5th order)	\hat{b}_i (4th order)
0			
$\frac{1}{5}$	$\frac{1}{5}$		
$\frac{3}{10}$	$\frac{3}{40}, \frac{9}{40}$		
$\frac{4}{5}$	$\frac{44}{45}, -\frac{56}{15}, \frac{32}{9}$		
$\frac{8}{9}$	$\frac{19372}{6561}, -\frac{25360}{2187}, \frac{64448}{6561}, -\frac{212}{729}$		
1	$\frac{9017}{3168}, -\frac{355}{33}, \frac{46732}{5247}, \frac{49}{176}, -\frac{5103}{18656}$		
1	$\frac{35}{384}, 0, \frac{500}{1113}, \frac{125}{192}, -\frac{2187}{6784}, \frac{11}{84}$	$\frac{35}{384}$	$\frac{5179}{57600}$
		0	0
		$\frac{500}{1113}$	$\frac{7571}{16695}$
		$\frac{125}{192}$	$\frac{393}{640}$
		$-\frac{2187}{6784}$	$-\frac{92097}{339200}$
		$\frac{11}{84}$	$\frac{187}{2100}$

Step Computation :

Initially, we evaluate the 7 functions and for each step $t_{n+1} = t_n + h$, we compute

the following intermediate values.

$$\left. \begin{aligned} k_1 &= f(t_n, y_n), \\ k_2 &= f\left[t_n + \frac{1}{5}h, y_n + \frac{1}{5}hk_1\right], \\ k_3 &= f\left[t_n + \frac{3}{10}h, y_n + h\left(\frac{3}{40}k_1 + \frac{9}{40}k_2\right)\right], \\ k_4 &= f\left[t_n + \frac{4}{5}h, y_n + h\left(\frac{44}{45}k_1 - \frac{56}{15}k_2 + \frac{32}{9}k_3\right)\right], \\ k_5 &= f\left[t_n + \frac{8}{9}h, y_n + h\left(\frac{19372}{6561}k_1 - \frac{25360}{2187}k_2 + \frac{64448}{6561}k_3 - \frac{212}{729}k_4\right)\right], \\ k_6 &= f\left[t_n + h, y_n + h\left(\frac{9017}{3168}k_1 - \frac{355}{33}k_2 + \frac{46732}{5247}k_3 + \frac{49}{176}k_4 - \frac{5103}{18656}k_5\right)\right], \\ k_7 &= f\left[t_n + h, y_n + h\left(\frac{35}{384}k_1 + \frac{500}{1113}k_3 + \frac{125}{192}k_4 - \frac{2187}{6784}k_5 + \frac{11}{84}k_6\right)\right]. \end{aligned} \right\} \quad (5.4)$$

Now we update the value of 5th order solution and 4th order error estimation with the help of values of k_i . The values of k_i 's obtained from equation (5.4) is used for calculating the 5th-order solution,

$$y_{n+1} = y_n + h\left(\frac{35}{384}k_1 + \frac{500}{1113}k_3 + \frac{125}{192}k_4 - \frac{2187}{6784}k_5 + \frac{11}{84}k_6\right). \quad (5.5)$$

The 4th-order embedded solution (for error estimation) is given as,

$$\hat{y}_{n+1} = y_n + h\left(\frac{5179}{57600}k_1 + \frac{7571}{16695}k_3 + \frac{393}{640}k_4 - \frac{92097}{339200}k_5 + \frac{187}{2100}k_6 + \frac{1}{40}k_7\right). \quad (5.6)$$

Error can be estimated as,

$$\text{Error} = \|y_{n+1} - \hat{y}_{n+1}\| \approx \mathcal{O}(h^5). \quad (5.7)$$

To keep the error within tolerance, we need to adjust h ,

$$h_{\text{new}} = h \cdot \left(\frac{\text{tol}}{\text{error}}\right)^{1/5}.$$

Convergence :

The local truncation error (LTE) is $O(h^6)$ (for 5th-order method) and the global error is given as $O(h^5)$ after $N \propto 1/h$ steps, and the calculated embedded error comes out to be $O(h^5)$, but is used to estimate the LTE of the 4th-order solution.

The Dormand-Prince 5(4) method combines high-order accuracy with robust step-size control, making it a standard for non-stiff ODEs. Its mathematical formulation ensures efficient error estimation.

5.2 DOP853

The Dormand-Prince 8(5, 3) method (called DOP853) is an embedded explicit Runge-Kutta method of 8th order with a 5th-order error estimator and 3rd-order dense output. It is designed for high-precision numerical integration of non-stiff ordinary differential equations (ODEs).

Consider an ordinary differential equation as given in equation (5.1).

The Runge-Kutta form is given as,

$$y_{n+1} = y_n + h \sum_{i=1}^s b_i k_i, \quad (5.8)$$

where, h is the step size, s is the number of stages (13 for DOP853), and k_i are the intermediate slopes.

Step Computation:

For $i = 1, 2, \dots, 13$,

$$k_i = f \left(t_n + c_i h, y_n + h \sum_{j=1}^{i-1} a_{ij} k_j \right). \quad (5.9)$$

The 8th-order solution is given as,

$$y_{n+1} = y_n + h \sum_{i=1}^{13} b_i k_i, \quad (5.10)$$

and the 4th-order embedded solution (for error control) is given as,

$$\hat{y}_{n+1} = y_n + h \sum_{i=1}^{13} b_i^* k_i. \quad (5.11)$$

Error can be estimated using,

$$\text{Error} = \|y_{n+1} - \hat{y}_{n+1}\| \approx \text{Local Truncation Error (LTE)}. \quad (5.12)$$

Convergence:

The primary method is 8th-order is given as,

$$y(t_{n+1}) - y_{n+1} = \mathcal{O}(h^9), \quad (5.13)$$

and the embedded method is 5th-order comes out to be,

$$y(t_{n+1}) - \hat{y}_{n+1} = \mathcal{O}(h^6). \quad (5.14)$$

The error estimator is of order $\mathcal{O}(h^6)$, which allows the adaptive step-size control. The values of c_i , a_{ij} , and b_i in equation (5.9) can be referred to from Hairer et al. [24].

5.3 Results

We modeled the baryonic discs from "The HI Nearby Galaxy Survey" Walter et al. [25] (THINGS) for which the data are publicly available, to estimate the 3-D distribution of HI. As a part of THINGS, a total of 34 galaxies were observed in the HI with the "Very Large Array" (VLA) with a high spatial resolution, Patra [26].

From the input data for atomic hydrogen, the variation of surface density with radius for HI is shown in the figure (5.1).

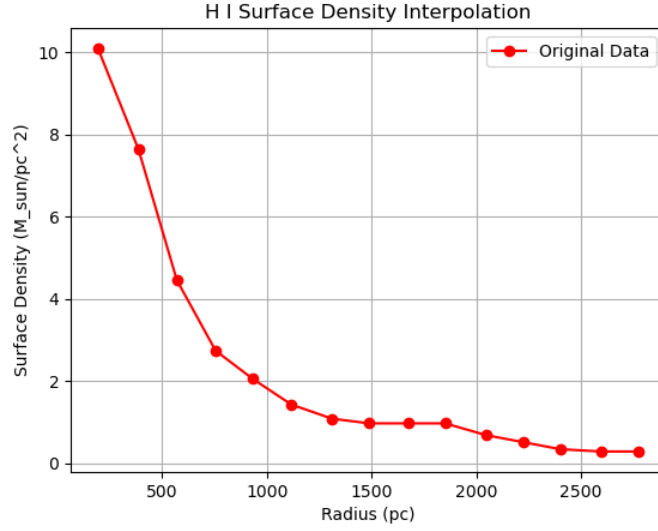


Figure 5.1: Plot of surface density vs radius for HI

The graph (5.1) illustrates the variation of the HI surface density as a function of galactocentric radius. For radii ≤ 500 pc, the surface density is relatively high due to the strong central concentration of HI in the galaxy. However, it gradually decreases toward the outer regions, particularly beyond (≥ 2000) pc.

From the observed data, the variation of surface density with radius for stars is shown in the figure (5.2). The plot shows that the stellar surface density exhibits a radial decline as one moves away from the galactic center. A significant amount of the stellar mass is concentrated near the central regions of the galaxy, and it progressively diminishes at larger radii. The reduction

in stellar mass distribution is a consequence of the decreasing gravitational force with increasing radial distance, and it becomes insufficient to confine the baryonic matter in the galaxy's outer regions.

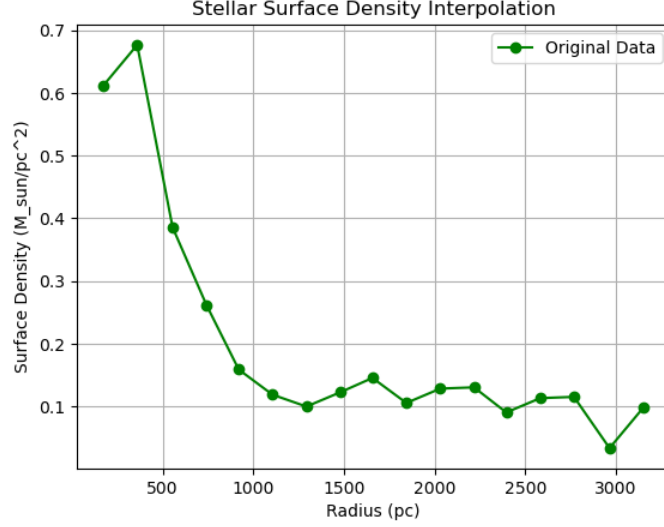


Figure 5.2: Plot of surface density vs radius for stars

The figure (5.3) shows the plot of the Milky Way galaxy for its density variation and height.

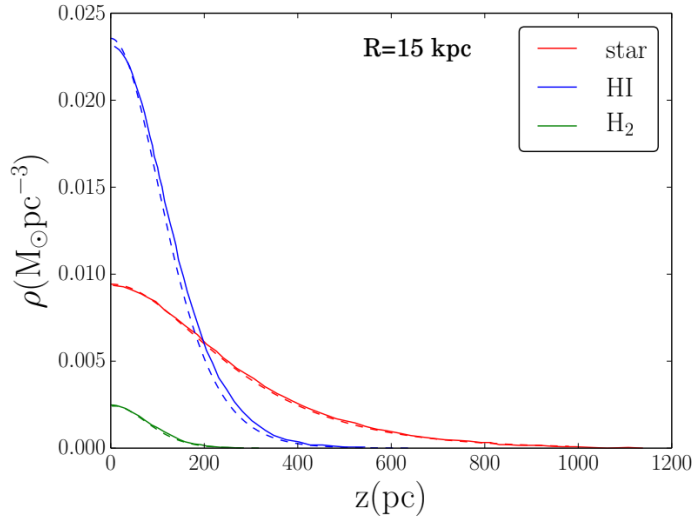


Figure 5.3: Plot of density vs height

We solve the equations (4.24) and (4.54) numerically to obtain the density as a function of height (z) at different values of R . The plot (5.3) shows

the vertical density distribution of stars, HI, and H_2 for $\sigma_{HI} = 7$ km/s and $a_0 = 1.2 \times 10^{-8}$ cm/s² at $R = 15$ kpc. As observed from the graph, the H_2 gas layer extends to 200 pc while stars and HI layers extend up to nearly 1000 pc and 420 pc, respectively.

The figure (5.4) shows the surface density profile of NGC-925 as a function of radius.

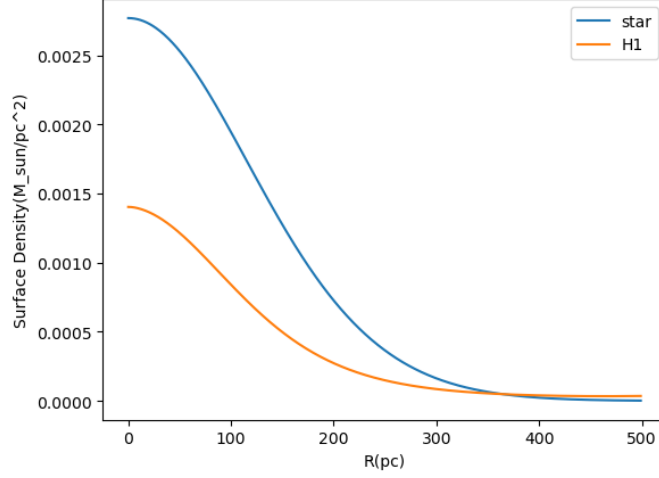


Figure 5.4: Plot of surface density vs R

The plot (5.4) illustrates the variation of surface density at $R = 700$ pc. Based on data from the THINGS survey, the stellar disk dominates the surface density in the inner regions, while HI becomes dominant in the outskirts. The stellar surface density exhibits significantly greater variation compared to that of HI, but both components ultimately show a decline in their surface densities with increasing radius.

Chapter 6

Conclusion

The thesis entitled "Investigating the Equation of Hydrostatic Equilibrium under the Modified Newtonian Dynamics" is devoted to studying the vertical structure of galactic discs by applying the MOND framework to the hydrostatic equilibrium of stars, atomic hydrogen, and molecular hydrogen. The study modeled the gravitational influence among the baryonic components by constructing and solving a set of coupled second-order differential equations.

As these equations are difficult to solve analytically, we implemented numerical methods to determine the scale height of the gas layers. The analysis shows that MOND can partially reproduce the flaring of HI gas in the outer galaxy, but it underpredicts the scale height in the intermediate radial range. Also, the inclusion of gas self-gravity in the inner part of the galaxy proved significant in shaping the vertical structure.

Overall, the results show that MOND is a viable alternative to dark matter for explaining certain features of galaxies' vertical structure. The work provides a basis for building refined models by considering the additional factors like the pressure from turbulence and magnetic forces, which encourages further study of MOND as a better theory for understanding galactic dynamics.

Future Scope

- Although the mass modeling has been carried out for the Milky Way galaxy, this work can be further extended to external galaxies such as NGC-6946 to test the applicability of the MOND framework in different galactic environments.
- Since we have access to the high-resolution data from the THINGS survey, it is possible to carry out detailed computations and compare the theoretical predictions with observational results and assess the consistency and robustness of the model.
- If the model demonstrates consistency with observational data, it may serve as a viable alternative to the dark matter theory in explaining certain structural features of galaxies, as evidenced by its application to the Milky Way.

Bibliography

- [1] Brada, R., & Milgrom, M. (1995). Exact solutions and approximations of MOND fields of disc galaxies. *Monthly Notices of the Royal Astronomical Society*, 276(2), 453-459.
- [2] Sanders, R. H. (2010). The dark matter problem: A historical perspective. *Cambridge University Press*.
- [3] Angus, G. W. (2016, May). The dynamics of face-on galaxies in MOND. *In Journal of Physics: Conference Series* (Vol. 718, No. 3, p. 032001).
- [4] Milgrom, M., & Bekenstein, J. (1987). The modified Newtonian dynamics as an alternative to hidden matter. *In Symposium-International Astronomical Union* (Vol. 117, pp. 319-333).
- [5] Milgrom, M. (1983). A modification of the Newtonian dynamics as a possible alternative to the hidden mass hypothesis. *Astrophysical Journal*, Part 1 (ISSN 0004-637X), vol. 270, July 15, 1983, p. 365-370.
- [6] Sanders, R. H. (2015). A historical perspective on modified Newtonian dynamics. *Canadian Journal of Physics*, 93(2), 126-138.
- [7] Pizagno, J., Prada, F., Weinberg, D. H., Rix, H. W., Pogge, R. W., Grebel, E. K., & Gunn, J. E. (2007). The Tully-Fisher relation and its residuals for a broadly selected sample of galaxies. *The Astronomical Journal*, 134(3), 945.

- [8] Milgrom, M. (2002). Does dark matter really exist? *Scientific American*, 287(2), 42-52.
- [9] De Blok, W. J. G., Walter, F., Brinks, E., Trachternach, C., Oh, S. H., & Kennicutt, R. C. (2008). High-resolution rotation curves and galaxy mass models from THINGS. *The Astronomical Journal*, 136(6), 2648.
- [10] Oort, J. H., & Woltjer, L. (1962). The Distribution and Motion of Interstellar Matter in Galaxies. *Astronomy & Astrophysics*, v.143, p. 3-22.
- [11] Dickey, J. M., & Lockman, F. J. (1990). HI in the Galaxy. IN: *Annual Review of Astronomy & Astrophysics*. Vol. 28 (A91-28201 10-90).
- [12] Scoville, N. Z., & Sanders, D. B. (1987). H_2 in the Galaxy. In *Interstellar Processes: Proceedings of the Symposium on Interstellar Processes*, pp. 21-50. *Springer Netherlands*.
- [13] Sanders, D. B., Solomon, P. M., & Scoville, N. Z. (1984). Giant molecular clouds in the Galaxy. The axisymmetric distribution of H_2 . *Astrophysical Journal*, Part 1 (ISSN 0004- 637X), vol. 276, Jan. 1, 1984, p. 182-203., 276.
- [14] Mera, D., Chabrier, G., & Schaeffer, R. (1998). Towards a consistent model of the Galaxy: II. Derivation of the model. *Astronomy & Astrophysics*, v.330, p.953-962.
- [15] Narayan, C. A., & Jog, C. J. (2002). Vertical scale heights in a gravitationally coupled, three-component Galactic disk. *Astronomy & Astrophysics*, 394(1), 89-96.
- [16] Lockman, F. J., & Gehman, C. S. (1991). Vertical distribution and support of galactic HI. *Astrophysical Journal*, Part 1 (ISSN 0004- 637X), vol. 382, Nov. 20, 1991, p. 182-188.

- [17] Sanders, R. H., & McGaugh, S. S. (2002). Modified Newtonian dynamics as an alternative to dark matter. *Annual Review of Astronomy and Astrophysics*, 40(1), 263-317.
- [18] Olling, R. P. (1996). The highly flattened dark matter halo of NGC 4244. *Astronomical Journal*, v.112, p.481.
- [19] Combes, F., & Becquaert, J. F. (1997). Vertical equilibrium of molecular gas in galaxies. *Astronomy & Astrophysics*, v.326, p.554-564.
- [20] Kalberla, P. M. W., Dedes, L., Kerp, J., & Haud, U. (2007). Dark matter in the Milky Way-II. The HI gas distribution as a tracer of the gravitational potential. *Astronomy & Astrophysics*, 469(2), 511-527.
- [21] Sánchez-Salcedo, F. J., Saha, K., & Narayan, C. A. (2008). The thickness of HI in galactic discs under Modified Newtonian Dynamics: theory and application to the Galaxy. *Monthly Notices of the Royal Astronomical Society*, 385(3), 1585-1596.
- [22] Bekenstein, J. D. (2006). The modified Newtonian dynamics—MOND and its implications for new physics. *Contemporary Physics*, 47(6), 387-403.
- [23] Milgrom, M. (2001). The shape of ‘dark matter’ haloes of disc galaxies according to MOND. *Monthly Notices of the Royal Astronomical Society*, 326(4), 1261-1264.
- [24] Hairer, E., Wanner, G, & Syvert P. Nørsett. (1993). Solving Ordinary Differential Equations. *Springer Series in Computational Mathematics*, ISSN 0179-3632.
- [25] Walter, F., Brinks, E., De Blok, W. J. G., Bigiel, F., Kennicutt, R. C., Thornley, M. D., & Leroy, A. (2008). THINGS: The HI nearby galaxy survey. *The Astronomical Journal*, 136(6), 2563.

- [26] Patra, N. N. (2020). HI scale height in spiral galaxies. *Monthly Notices of the Royal Astronomical Society*, 499(2), 2063-2075.